Support Information

Dipole orientation-induced Interfacial energy level alignment difference in 2D perovskite passivated 3D perovskite by in-situ investigation

Ruifeng Zheng[1+], Jielei Li[1+], Shengwen Li[1]*, Bingchen He[1], Shi Chen[1]*

[1]Institute of Applied Physics and Materials Engineering, University of Macau, Macau SAR 999078, P. R. China.

Corresponding authors: shengwenli@um.edu.mo, shichen@um.edu.mo

+ These authors contributed equally.

Keywords: Interfacial energetics; 2D perovskite; passivation; in-situ; perovskite solar cell.

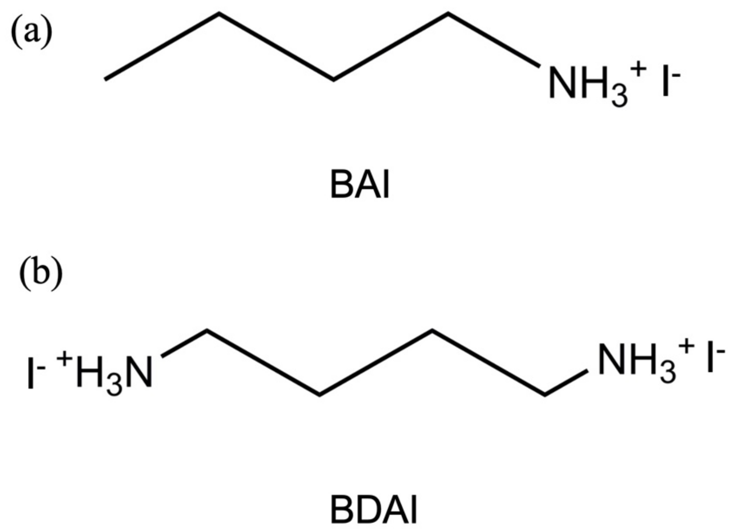

Figure S1. Chemical structures of (a) BAI and (b) BDAI

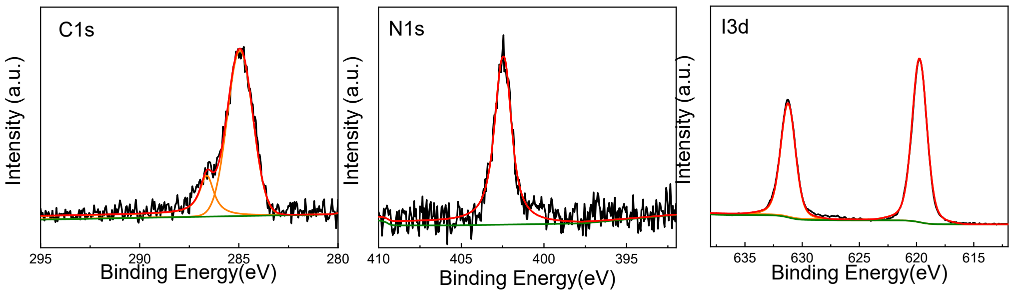

Figure S2. XPS spectra of BAI grown on ITO substrate.

	C-C	C-N	N1s	I3d
Area	2907	987	1748	25758
Normalized	9820	3334	3665	4151
Ratio	2.95	1.00	1. 10	1.25

Table S1. The calculated content ratio of BAI grown on ITO substrate.

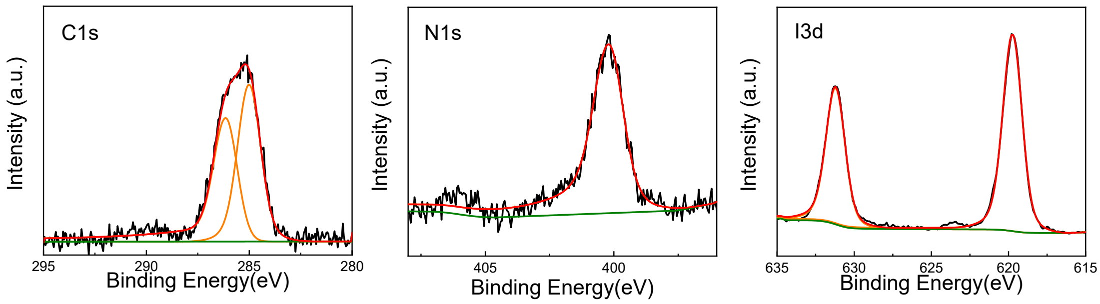

Figure S3. XPS spectra of BDAI grown on ITO substrate.

	C-C	**C-N**	**N1s**	**I3d**
Area	2800	2796	4359	73766
Normalized	9459	9444	9139	11886
Ratio	1.00	1.00	0.97	1.26

Table S2. The calculated content ratio of BDAI grown on ITO substrate.

	C-N	C-C	N
pristine	1	0.81	0.91
0.5nm	1	1.08	1.04
1nm	1	1.08	1.01
2nm	1	1.13	0.99
4nm	1	1.21	0.91
6nm	1	1.27	0.88
8nm	1	1.30	0.85
16nm	1	1.72	0.89
32nm	1	2.70	0.91

Table S3. The calculated content ratio of BAI grown on PSK substrate.

	C-N	C-C	N
pristine	1	1.35	0.96
1nm	1	1.16	0.89
2nm	1	1.17	0.87
4nm	1	1.19	0.87
8nm	1	1.19	0.85
20nm	1	1.25	0.86

Table S4. The calculated content ratio of BDAI grown on PSK substrate.

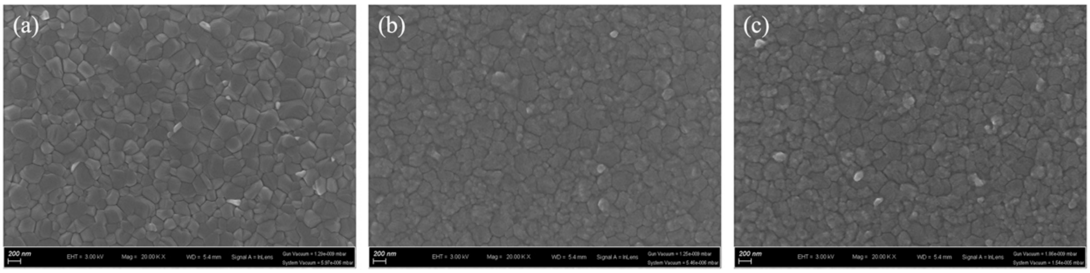

Figure S4 SEM images of (a) pristine perovskite film and perovskite films deposited with (b) BAI and (c) BDAI

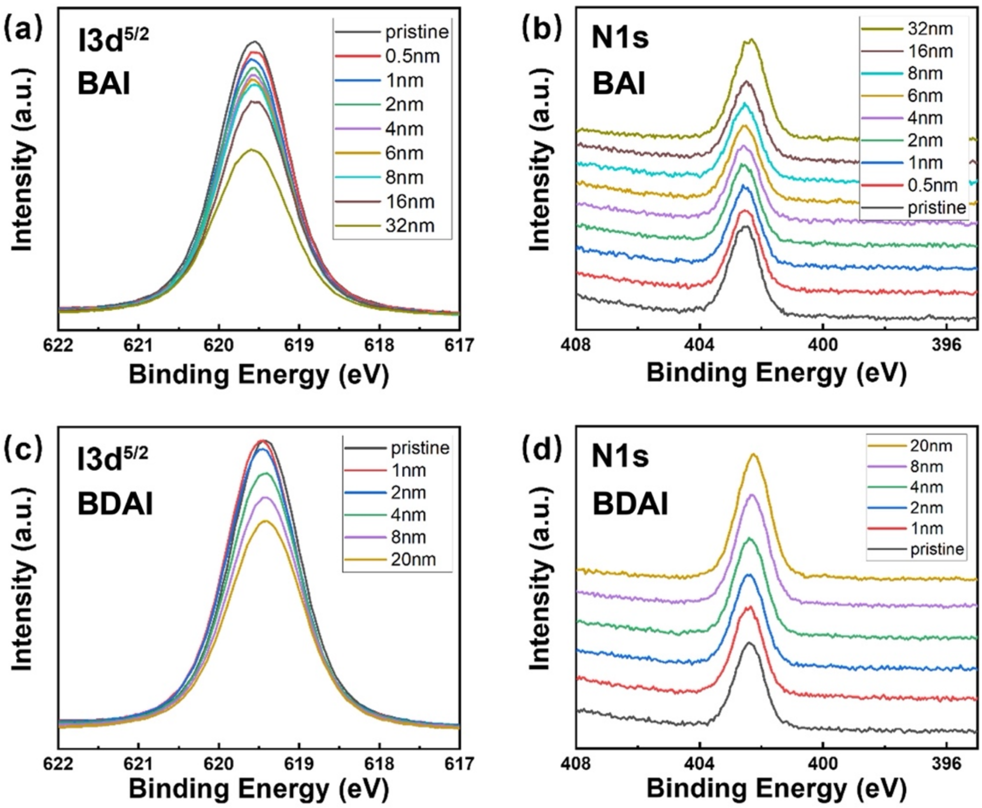

Figure S5. (a,b) XPS images of BAI grown on perovskite substrates; (c,d) XPS images of BDAI grown on perovskite substrates.

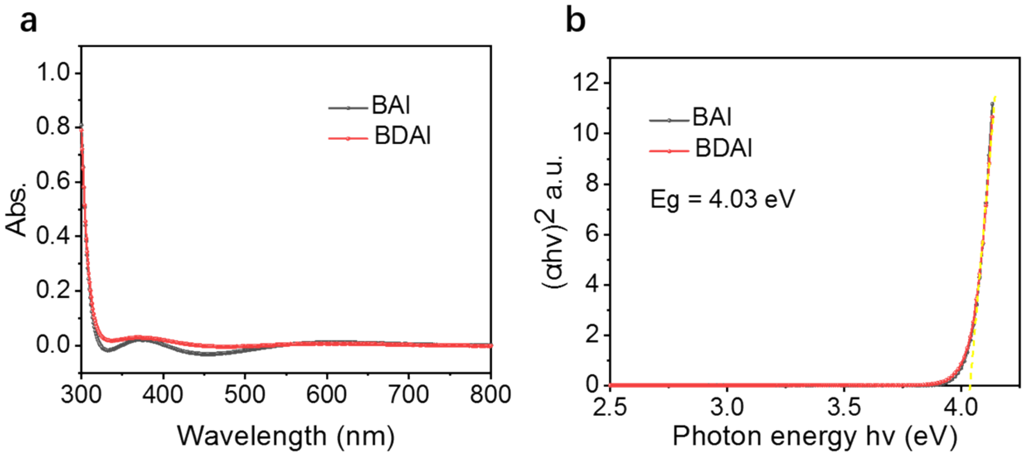

Figure S6, (a) UV-Vis measurement of BAI and BDAI molecular thin films on quartz; (b) calculated band gap for both molecules.

Measurements(nm)	Calculated(nm)
0	0
0.5	2.03
1	1.82
2	3.10
4	5.94
6	7.66
8	9.32
16	14.24

Table S5. Comparison of film thickness of BAI on PSK

Measurements(nm)	Calculated(nm)
0	0
1	0.13
2	1.21
4	4.48
8	9.56
20	19.18

Table S6. Comparison of film thickness of BDAI on PSK

Molecule	Structure	Perovskite	V_{OC} (V)	J_{SC} (mA/cm^2)	FF (%)	PCE (%)	Ref.
BAI	regular	$FAPbI_3$	1.16	24.95	81.23	23.46	[1]
BAI	regular	$Cs_{0.07}Rb_{0.03}FA_{0.765}MA_{0.135}PbI_{2.55}Br_{0.45}$	1.20	24.19	77.56	22.50	[2]
BAI	regular	$(FAPbI_3)_{0.95}(MAPbBr_3)_{0.05}$	1.15	22.69	78.90	20.67	[3]
BAI	regular	$MA_{0.1}FA_{0.9}PbI_{2.9}Br_{0.1}$	1.15	24.93	76.49	22.01	[4]
BAI	regular	$(FAPbI_3)_{0.95}(MAPbBr_3)_{0.05}$	1.11	23.99	81.70	21.71	[5]
BAI	inverted	$(AA)_2MA_4Pb_5I_{16}$	1.19	18.45	79.20	17.39	[6]
BAI	inverted	$FA_{0.25}MA_{0.75}PbI_3$	1.05	24.32	79.28	20.27	[7]
BAI	regular	$FAPbI_3$	1.18	24.72	79.27	23.13	[8]
BAI	regular	$Cs_{0.05}MA_{0.05}FA_{0.9}PbI_3$	1.16	26.01	83.90	25.32	[9]
BAI	regular	$CsPbI_3$	1.23	20.25	81.50	20.23	[10]
BAI	inverted	$Cs_{0.05}(FA_{0.92}MA_{0.08})_{0.95}Pb(I_{0.92}Br_{0.08})_3$	1.15	22.30	80.70	20.70	[11]
BDAI	inverted	$Cs_{0.15}FA_{0.85}Pb(I_{0.95}Br_{0.05})_3$	1.15	24.51	82.10	23.10	[12]
BDAI	inverted	$(Cs_{0.05}MA_{0.16}FA_{0.79})Pb(I_{0.84}Br_{0.16})_3$	0.99	26.92	78.87	20.99	[13]
BDAI	inverted	$(AA)_2MA_4Pb_5I_{16}$	1.24	18.69	79.13	18.34	[6]
BDAI	inverted	$(CsPbI_3)_{0.05}(FA_{0.85}MA_{0.15}Pb(I_{0.85}Br_{0.15})_3)_{0.95}$	1.21	22.59	81.63	22.31	[14]
BDAI	inverted	$Cs_{0.1}MA_{0.09}FA_{0.81}PbCl_{0.14}I_{2.86}$	1.04	24.50	79.90	20.50	[15]
BDAI	regular	$Cs_{0.05}(FA_{0.83}MA_{0.17})_{0.95}Pb(I_{0.83}Br_{0.17})_3$	1.13	24.10	74.60	20.32	[16]

Table S7. The device structure and photoelectric properties of PSCs passivated with BAI and BDAI in recent years.

Reference:

1 Wang, J. *et al.* Ambient air processed highly oriented perovskite solar cells with efficiency exceeding 23% via amorphous intermediate. *Chemical Engineering Journal* **446**, 136968 (2022).

2 Mahmud, M. A. *et al.* In situ formation of mixed-dimensional surface passivation layers in perovskite solar cells with dual-isomer alkylammonium cations. *Small* **16**, 2005022 (2020).

3 Zhao, X. *et al.* Effect of steric hindrance of butylammonium iodide as interface modification materials on the performance of perovskite solar cells. *Solar RRL* **6**, 2200078 (2022).

4 Jiang, X. *et al.* Deeper insight into the role of organic ammonium cations in reducing surface defects of the perovskite film. *Angewandte Chemie International Edition* **61**, e202115663 (2022).

5 Kim, H. *et al.* Optimal interfacial engineering with different length of alkylammonium halide for efficient and stable perovskite solar cells. *Advanced Energy Materials* **9**, 1902740 (2019).

6 Li, K. *et al.* High Efficiency Perovskite Solar Cells Employing Quasi-2D Ruddlesden-Popper/Dion-Jacobson Heterojunctions. *Advanced Functional Materials* **32**, 2200024 (2022).

7 Rana, T. R. *et al.* Scalable Passivation Strategies to Improve Efficiency of Slot Die-Coated Perovskite Solar Cells. *ACS Energy Letters* **9**, 1888-1894 (2024).

8 Lou, Q. *et al.* Room Temperature Ionic Liquid Capping Layer for High Efficiency FAPbI3 Perovskite Solar Cells with Long-Term Stability. *Advanced Science* **11**, 2400117 (2024).

9 Yang, W. *et al.* Visualizing interfacial energy offset and defects in efficient 2D/3D heterojunction perovskite solar cells and modules. *Advanced Materials* **35**, 2302071 (2023).

10 Du, Y. *et al.* Manipulating the formation of 2D/3D heterostructure in stable high-performance printable CsPbI3 perovskite solar cells. *Advanced Materials* **35**, 2206451 (2023).

11 Zhang, C. *et al.* Constructing a stable and efficient buried heterojunction via halogen bonding for inverted perovskite solar cells. *Advanced Energy Materials* **13**, 2203250 (2023).

12 Liu, S. *et al.* Effective passivation with size-matched alkyldiammonium iodide for high-performance inverted perovskite solar cells. *Advanced Functional Materials* **32**, 2205009 (2022).

13 Chang, H. W., Li, C. C., Haung, T. Y., Li, H. C. & Tan, C. S. Enhancing perovskite solar cell efficiency and stability through the incorporation of BDAI 2 and DMPDAI 2. *Energy Advances* **3**, 552-557 (2024).

14 Wu, S. *et al.* Modulation of defects and interfaces through alkylammonium interlayer for efficient inverted perovskite solar cells. *Joule* **4**, 1248-1262 (2020).

15 Tien, C.-H., Lai, W.-S. & Chen, L.-C. Buried Interface Passivation Using Organic Ammonium Salts for Efficient Inverted CsMAFA Perovskite Solar Cell Performance. *ACS omega* **9**, 23033-23039 (2024).

16 Wang, X. *et al.* Interfacial modification via a 1, 4-butanediamine-based 2D capping layer for perovskite solar cells with enhanced stability and efficiency. *ACS Applied Materials & Interfaces* **14**, 22879-22888 (2021).